Dual Mass Spectrometric Tissue Imaging of Nanocarrier Distributions and their Biochemical Effects

Kristen N. Sikora, Joseph M. Hardie, Laura J. Castellanos-García, Yuanchang Liu, Biidaaban Reinhardt, Michelle E. Farkas, Vincent M. Rotello, Richard W. Vachet*

Corresponding Author
*Richard W. Vachet: e-mail, rwvachet@chem.umass.edu; phone, (+1) 413-545-2733; fax, (+1) 413-545-4490.
Department of Chemistry, University of Massachusetts, Amherst, Massachusetts 01003, United States

Table of Contents

Chemicals and Materials. 2,5-dihydroxybenzoic acid (DHB), arginine, 1-pentanthiol, and linoleic acid were purchased from Sigma-Aldrich (St. Louis, MO). Chloroauric acid for gold nanoparticle synthesis was bought from Strem Chemicals Inc. (Newburyport, MA). siRNA targeting TNF-α with the sequence: 5′-GUCUCAGCCUCUUCUCAUUCCUGct-3′ (sense strand) was synthesized by Sigma-Aldrich. Scramble siRNA with the sequence: 5′-UUCUCCGAACGUGUCACGU-3′ (sense strand) was purchased from Life Technologies (Carlsbad, CA). Phosphate-buffered saline (PBS) was purchased from Fisher Scientific. Indium tin oxide (ITO) conductive slides were purchased from Delta Technologies (Loveland, CO). All other chemicals were purchased from Sigma-Aldrich or Fisher Scientific and used as received unless otherwise specified.

Nanoparticle and NPSC Synthesis. Arginine-functionalized AuNPs (Arg-AuNPs) and NPSCs were synthesized according to a previous report.[1] In brief, 1-pentanethiol protected AuNPs (Au-C5) with ~2 nm core diameters were synthesized using the Brust-Sciffrin two-phase synthesis.[2] Arginine-functionalized thiol ligands were synthesized based on a previous report.[3] They were then conjugated to the AuNP core by the Murray place-exchange method.[4] To form the NPSCs, 1 μL linoleic acid was combined with 1 μM Arg-AuNPs in PBS. Emulsions were formed by using an amalgamator at 5000 rpm for 100 s. 10 μL of the emulsion was combined with a mixture of 2.5 μM Arg-AuNPs and 1 μM siRNA (90 μL in 5 mM phosphate buffer). The mixture was incubated for 10 min at room temperature.

Animal Experiments and Tissue Section Preparation. All animal protocols were approved by the University of Massachusetts Amherst Institutional Animal Care and Use Committee (IACUC), which is guided by the U.S. Animal Welfare Act and U.S. Public Health Service Policy. Female Balb/c mice (8-week-old) were obtained from Charles River Laboratories, Inc. (Wilmington, MA) and housed in controlled climates (22 ± 2 °C temperature, 12 h light/dark daily cycle) with free access to food and water. The mice were randomly divided into control and treated groups. Each was injected with 200 μL of either PBS or 2.5 μM of NPSCs via the tail vein. After 48 h, mice were

sacrificed via carbon dioxide inhalation and cervical dislocation. Mouse tissues were immediately extracted, flash frozen in liquid nitrogen, and then kept at -80 °C until used for MS imaging. Using a LEICA CM1850 cryostat, flash-frozen spleen tissues were sliced to 12 μm, thaw-mounted onto ITO slides (MALDI-MS) or glass slides (LA-ICP-MS) and desiccated under vacuum for 1 h. For the MALDI-MS imaging experiments, a Bruker ImagePrep apparatus was used to spray a 25 mg/mL 2,5-DHB solution (1:1 methanol:water) onto the tissues.

Pixel Counting and Analysis for Overlaid Images. Overlaid images (Figures 3, 4, 5, and 6) were converted into their individual RGB values using ImageJ. On an RGB scale of 0-255, we found that pixels outside of the tissue region consistently had individual RGB values below 40, so we set a background cutoff at this value for all tissues and all filters. To obtain the yellow pixels, each individual red pixel was multiplied by each individual green pixel (i.e. red x green = yellow). To determine the number of overlaid yellow pixels, we simply counted those pixels with values between 10,200 (i.e. 40 x 255) and 65,025 (255 x 255). Anything below the threshold of 10,200 was considered a non-colocalized pixel. The total number of yellow (overlaid) pixels was then divided by the number of red or green pixels, depending on the image and comparison set, to determine the percent of overlap between the analytes of interest.

Table S-1. ICP-MS analyses of TNF-α and scrambled NPSC-injected mouse tissues. All concentrations are reported as the average among three mice. Error is reported as standard deviation.

Tissue Type	Gold Concentration for TNF-α NPSC mice (ppb)	Gold Concentration for Scrambled NPSC mice (ppb)
Spleen	26000 ± 2000	20000 ± 3000
Liver	23000 ± 3000	20000 ± 3000
Kidney	220 ± 20	310 ± 10
Lung	3500 ± 900	3000 ± 400
Heart	900 ± 500	890 ± 200
Blood	150 ± 40	70 ± 40
Small Intestine	90 ± 20	160 ± 20
Brain	10 ± 1	20 ± 10

Table S-2. All detected analyte peaks, their adducts, and their identities.

Identity	m/z	Adduct	Identity	m/z	Adduct
GPC	258.1	[M + H+]	PE (p-40:5)	671.5	[M – HG + K+]
CAR (16:0)	400.4	[M + H+]	2H Cer (d18:1/25:1)	681.7	[M + NH4+]
CAR (18:1)	426.6	[M + H+]	PC (30:0)	706.6	[M + H+]
LPC (16:0)	496.3 518.4	[M + H+] [M + Na+]	PE (p-36:4)	724.5	[M + Na+]
PE (26:4)	497.2	[M – HG + K+]	PE (p-34:1)	732.5	[M + H+]
LPC (p-18:0)	508.6	[M + H+]	PC (32:0)	734.5 772.5	[M+H+] [M + K+]
LPC (18:2)	520.2	[M + H+]	SM (d18:1/17:0)	741.6 757.6	[M + Na+] [M + K+]
LPC (18:0)	524.4	[M + H+]	PC (p-34:1)	744.6	[M + H+]
LPC (20:4)	544.3	[M + H+]	PC (p-34:0)	746.6	[M + H+]
PE (p-34:3)	557.5	[M – HG + H+]	PC (p-32:0)	756.5	[M + Na+]
PE (p-34:2)	559.5 581.5	[M – HG + H+] [M – HG + Na+]	PC (34:3)	756.6	[M + H+]
Cer(d18:1/18:1)	564.6	[M + H+]	SM (d18:1/20:0)	759.6	[M + H+]
PE (p-34:1)	583.5	[M – HG + H+]	PC (34:1)	760.6 782.6 798.6	[M + H+] [M + Na+] [M + K+]
PE (p-36:4)	583.5	[M – HG + Na+]	PC (34:0)	762.6	[M + H+]
PE (p-36:3)	585.5	[M – HG + H+]	PC (p-36:2)	770.6 792.6 808.5	[M + H+] [M + Na+] [M + K+]
Heme B	616.5 655.5	[M+H+] [M + K+]	SM (d18:1/21:1)	771.6 809.6	[M + H+] [M + K+]
2H Cer (d18:1/20:1)	632.5	[M + K+]	PC (34:2)	780.5	[M + Na+]
2H OH Cer (d18:1/20:0)	632.5 650.5	[M – H2O + K+] [M + K+]	PC (p-36:5)	786.6 802.5	[M + Na+] [M + K+]
GCer (d18:1/12:0)	666.5 682.5	[M + Na+] [M + K+]	PC (p-36:4)	788.6 804.5	[M + Na+] [M + K+]
PE (38:2)	669.5	[M – HG + K+]	PC (36:0)	790.6 812.6 828.5	[M + H+] [M + Na+] [M + K+]
PE (38:1)	671.5	[M – HG + K+]	PC (p-38:6)	790.6 812.6 828.5	[M + H+] [M + Na+] [M + K+]

Identity	m/z	Adduct
PC (p-38:5)	792.5 830.5	[M+H+] [M + K+]
PC (p-38:4)	794.7 816.6 832.5	[M + H+] [M + Na+] [M + K+]
PC (34:2)	796.5	[M + K+]
SM (d18:1/24:3)	809.6 847.6	[M + H+] [M + K+]
SM (d18:1/23:2)	819.6	[M + Na+]
PC (p-40:5)	820.6 858.6	[M + H+] [M + K+]
PC (p-40:0)	852.6	[M + Na+]
SM (d18:1/24:0)	853.7	[M + K+]
Ganglioside GM3 (d18:1/18:1(11Z))	1201.7	[M + Na+]
Angiotensin	1334.6	[M + K+]

Abbreviations: GPC – Glycerophosphocholine; LPC – lysophosphatidylcholine; PC – phosphatidylcholine; Cer – ceramide; GCer – Glucosylceramide; SM – sphingomyelin; PE – phosphatidylethanolamine; CAR – carnitine; “p-” – plasmalogen

Table S-3. Characteristic lipid ions in the spleen of scrambled NPSC-injected mice.

Lipid I.D.[a]	Detected m/z	Ion(s)	(+) or (-) in Scrambled NPSC-Injected Mouse Tissue	ROC AUC[c]	Change a Predicted Increase/Decrease for TNF NPSCs?
LPC (16:0)	496.3 518.4	$[M + H^+]$ $[M + Na^+]$	None	0.484 0.542	No
LPC (18:0)	524.4	$[M + H^+]$	None	0.515	No
LPC (p-18:0)	508.6	$[M + H^+]$	-	-	N/A
LPC (18:2)	520.2	$[M + H^+]$	None	0.553	No
LPC (20:4)	544.3	$[M + H^+]$	None	0.488	No
PC (30:0)	706.6	$[M + H^+]$	None	0.515	No
PC (32:0)	734.5 772.5	$[M + H^+]$ $[M + K^+]$	None	0.590 0.504	No
PC (p-32:0)	756.5	$[M + Na^+]$	(+)	0.652	Yes
PC (34:0)	762.6	$[M + H^+]$	(+)	0.773	Yes
PC (p-34:0)	746.6	$[M + H^+]$	(+)	0.686	Yes
PC (34:1)	760.6 798.6	$[M + H^+]$ $[M + K^+]$	None	0.501	No
PC (p-34:1)	744.6	$[M + H^+]$	(+)	0.683	No
PC (34:2)	780.5	$[M + Na^+]$	None	0.478	No
PC (34:3)	756.6	$[M + H^+]$	(+)	0.682	No
PC (p-36:5)	786.6 802.5	$[M + Na^+]$ $[M + K^+]$	None	0.482 0.604	No
PC (p-36:4)	788.6 804.5	$[M + Na^+]$ $[M + K^+]$	(+)	0.689 0.688	Yes
PC (p-36:2)	770.6 792.6 808.5	$[M + H^+]$ $[M + Na^+]$ $[M + K^+]$	None	N/A N/A 0.510	No
PC (36:0)[d]	790.6 812.6 828.5	$[M + H^+]$ $[M + Na^+]$ $[M + K^+]$	(+)	0.785 0.708 0.652	Yes
PC (p-38:6)[d]	790.6 812.6 828.5	$[M + H^+]$ $[M + Na^+]$ $[M + K^+]$	(+)	0.785 0.708 0.652	Yes
PC (p-38:5)	792.5 830.5	$[M + H^+]$ $[M + K^+]$	None	N/A 0.490	No
PC (p-38:4)	794.7 816.6 832.5	$[M + H^+]$ $[M + Na^+]$ $[M + K^+]$	-	-	N/A
PC (p-40:5)	820.6 858.6	$[M + H^+]$, $[M + K^+]$	None	0.426	No

2H OH Cer (d18:1/20:0)	632.5 650.5	[M – H_2O + K^+] [M + K^+]	None	0.575 0.437	No
2H Cer (d18:1/25:1)	681.7	[M + NH_4^+]	None	0.527	No
2H Cer (d18:1/20:1)	632.5	[M + K^+]	None	0.565	No
SM (d18:1/17:0)	741.6 757.6	[M + Na^+] [M + K^+]	None	0.479 0.635	No
SM (d18:1/20:0)	759.6	[M + H^+]	None	0.627	No
SM (d18:1/21:1)	771.6 809.6	[M + H^+] [M + K^+]	(+)	0.689 0.673	Yes
SM (d18:1/23:2)	819.6	[M + Na^+]	None	0.627	No
SM (d18:1/24:0)	853.7	[M + K^+]	-	-	N/A
SM (d18:1/24:3)	809.6 847.6	[M + H^+] [M + K^+]	(+)	0.798 0.777	No
PE (26:4)	497.2	[M – HG + K^+]	(+)	0.669	Yes
PE (p-34:3)	557.5	[M – HG + H^+]	None	0.531	No
PE (p-34:2)	559.5 581.5	[M – HG + H^+] [M – HG + Na^+]	None	N/A 0.583	No
PE (p-34:1)[d]	583.5	[M – HG + H^+]	None	0.468	No
PE (p-36:4)[d]	583.5	[M – HG + Na^+]	None	0.468	No
PE (p-34:1)	732.5	[M + H^+]	None	0.523	No
PE (p-36:4)	724.5	[M + Na^+]	None	0.469	No
PE (p-36:3)	585.5	[M – HG + H^+]	None	0.626	No
PE (38:2)	669.5	[M – HG + K^+]	-	-	N/A
PE (38:1)[d]	671.5	[M – HG + K^+]	None	0.583	No
PE (p-40:5)[d]	671.5	[M – HG + K^+]	None	0.583	No
CAR (16:0)	400.4	[M + H^+]	None	0.508	No
CAR (18:1)	426.6	[M + H^+]	None	0.420	No

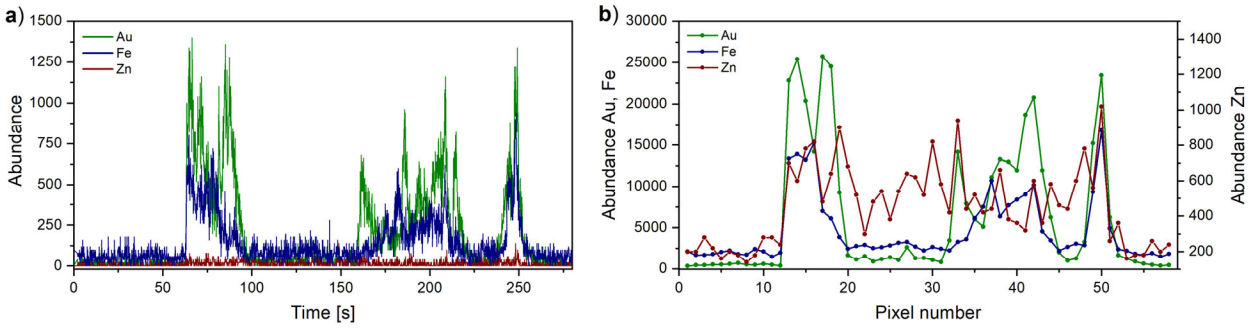

Figure S-1. Data reduction process to produce pixels for each line of data obtained from LA-ICP-MS experiments. (a) Example raw LA-ICP-MS data for gold (Au), iron (Fe), and zinc (Zn) obtained from a single line scan of the tissue of interest, with the indicated time representing the time after the 15 µm/s laser scan begins. (b) The raw data is converted into pixelated data by binning 33 data points to generate a single 50 µm x 50 µm pixel, as represented by each data point. Tissue edges can be identified by the shift from noise to signal at ~60 seconds and the shift from signal to noise at ~260 seconds.

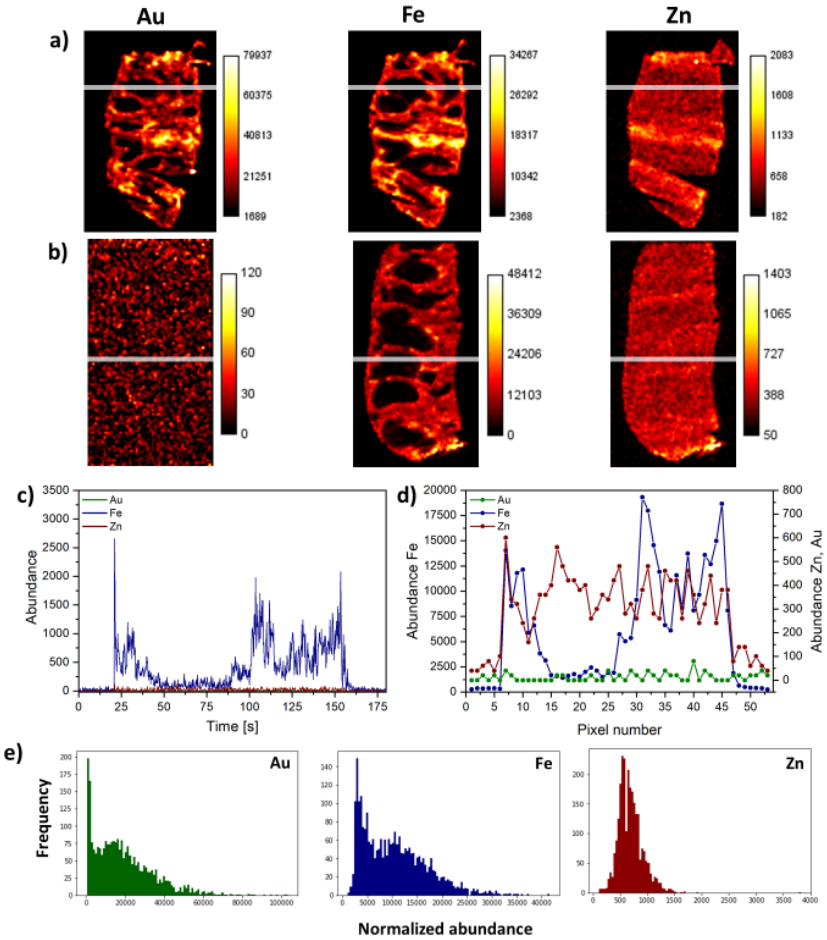

f)

Tissue signal average			
Metal	Average	Std	% deviation
Au	18903	15410	81
Fe	10404	6487	62
Zn	694	231	33

Figure S-2. LA-ICP-MS image generation and signal analysis for NPSC-injected and control mouse spleen. Raw images obtained for Au, Fe, and Zn for (a) NPSC-injected and (b) control mouse spleen tissues were generated using the method described in the main text and in Figure S-1. (c) Example raw data for the line indicated in the control tissue shown in (b), displaying the signals for Au, Fe, and Zn as function of time after beginning the laser scan. (d) Example binned data from the same control tissue in (c). It can be seen from the abundances of elements in both Figures S-1 and (c & d) that Zn remains relatively constant over the entirety of the tissue. (e) Example histograms for the intensity distributions for Au, Fe, and Zn throughout the entire tissue for the NPSC-injected tissue slice shown in (a). Au and Fe both have two broad distributions, whereas Zn only has one narrow one, which is consistent with it having a relatively constant distribution across the tissue. (f) Averages and standard deviations for the Au, Fe, and Zn signals shown in (e).

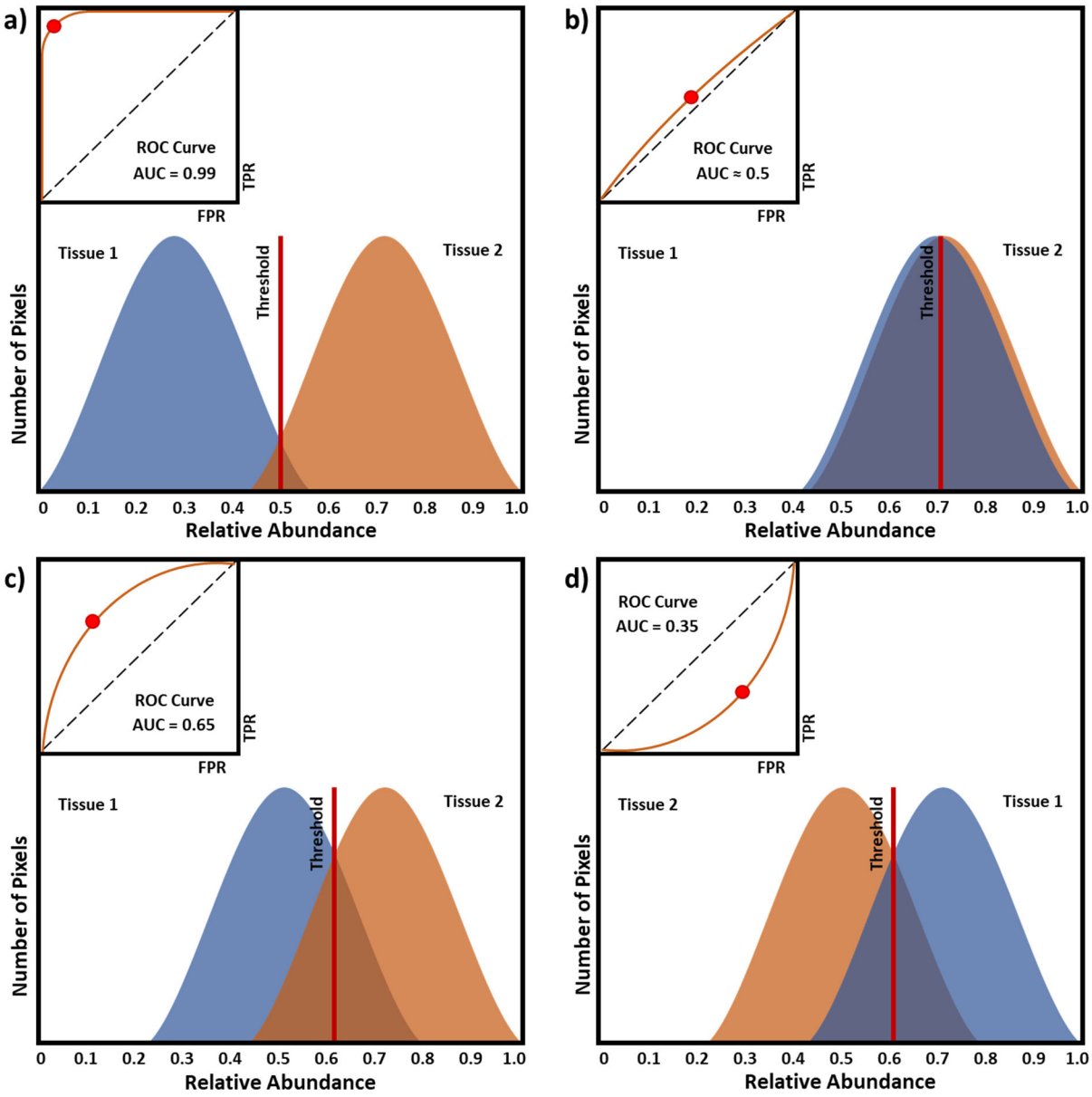

Figure S-3. Example ROC curves for theoretical data, illustrating the statistical meaning of the area under the curve (AUC) values. Tissue 1 and 2 are arbitrarily selected; for our analyses, “Tissue 1” represents the control tissue and “Tissue 2” represents the NPSC-treated tissue. The Gaussians represent the signal abundance distributions for each tissue type (x-axis) at a selected m/z value. The y-axis represents the number of pixels found at each abundance threshold. For example, in (a) if the threshold is set to 50% relative abundance, there are approximately half of the total pixels correlated to Tissue 1 below the threshold and half of the total pixels correlated to Tissue 2 above the threshold, making this particular m/z value is a successful classifier for the two tissue types. In (b), at a threshold of 70% relative abundance, there are almost an equal number of pixels correlated to Tissue 1 and Tissue 2 both above and below the threshold, indicating that

this m/z value is not a viable classifier for the two tissue types. The ROC curve is formed by plotting the coordinates for the true positive rates (TPR) (i.e. the number of Tissue 2 pixels found above the threshold, divided by the total number of Tissue 2 pixels) versus the false positive rates (FPR) (i.e. the number of Tissue 1 pixels found above the threshold, divided by the total number of Tissue 1 pixels) for every threshold (red line in each graph) across the relative signal abundancies ranging from 0% to 100% Each point on an ROC curve is the result of the FPR vs. TPR for each set threshold point. The area under the ROC curve (AUC) that results from this analysis is used to assess the validity of the m/z as a distinctive biomarker between the two tissue types. (a) For tissues with distinguishable Gaussian distributions, the false positive rate (FPR) will remain low as the true positive rate (TPR) increases because there is very little overlap in their relative abundancies. An ROC AUC close to 1 indicates that a given m/z value is able to successfully classify Tissue 2 when compared to Tissue 1. (b) An ROC AUC close to 0.5 indicates that the m/z value is not able to distinguish Tissue 2 from Tissue 1 and cannot be used as a binary classifier. (c) An ROC AUC greater than 0.65 typically indicates that the abundance distribution of a given m/z value is significantly increased in Tissue 2 as compared to Tissue 1. (d) An ROC AUC less than 0.35 typically indicates that the abundance distribution of a given m/z value is significantly decreased in Tissue 2 as compared to Tissue 1.

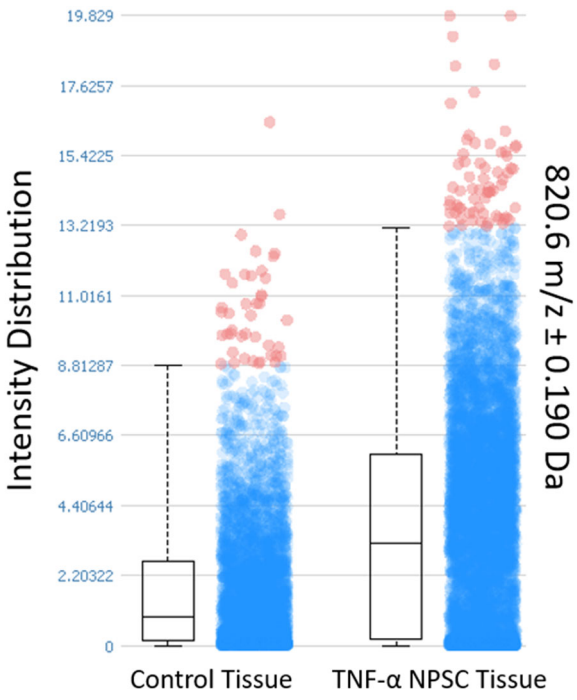

Figure S-4. Example ion abundance box-and-whisker plot of m/z 820.6 (PC (p-40:5) + H^+). The highest and lowest bars represent the maximum distribution, while the upper, middle, and lower lines of the box represent first quartile, median, and third quartile, respectively. Analytes that have greater medians for NPSC-injected mice were considered significantly different.

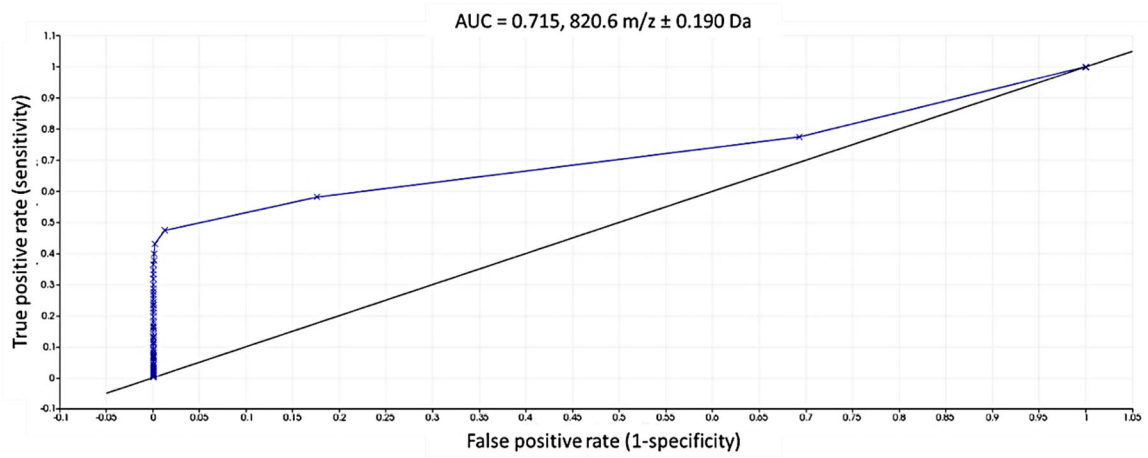

Figure S-5. Acquired ROC curve for m/z 820.6 (PC (p-40:5) + H^+). An ROC AUC of 0.715 indicates that m/z 820.6 is significantly different in intensity between the control and NPSC-injected mouse tissues.

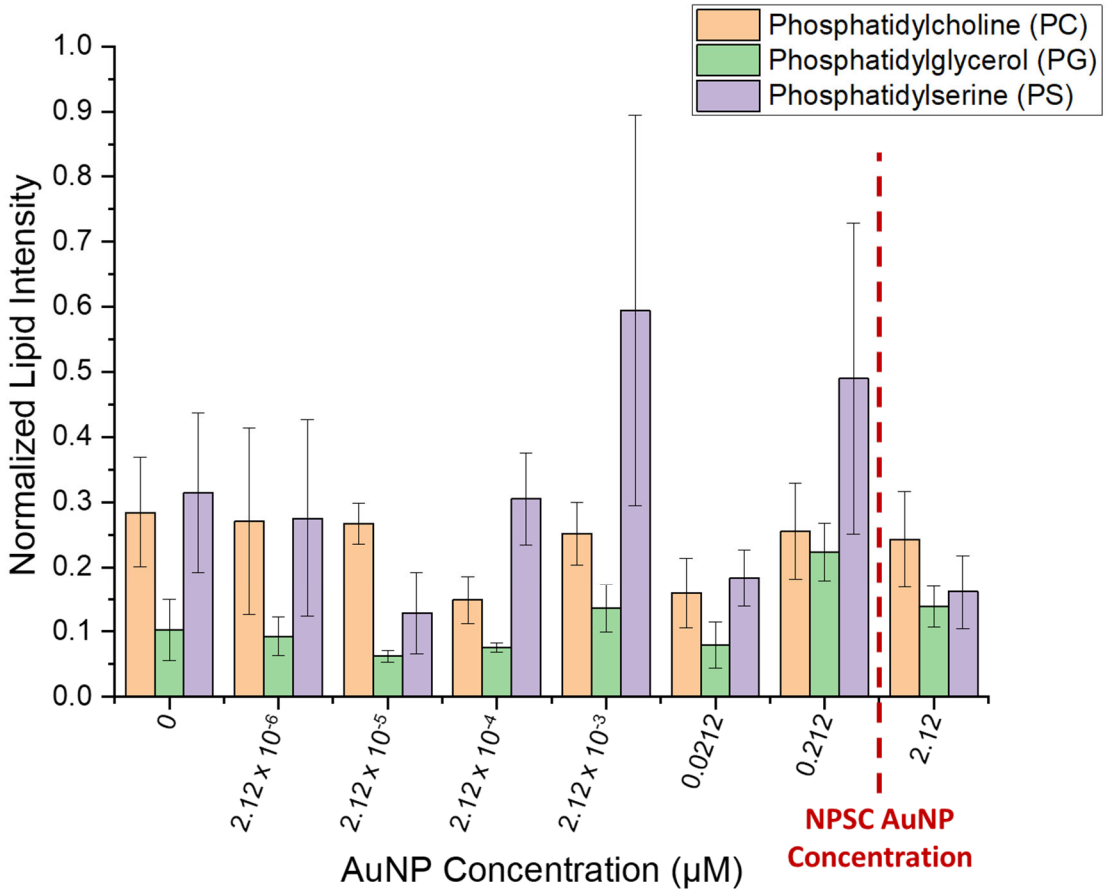

Figure S-6. MALDI-MS signal of lipids in the presence of AuNPs. Representative lipids of different polarities (positive – PC; neutral – PG; negative – PS) were measured in combination with DHB as a matrix and increasing concentrations of AuNPs. Lipid intensities were normalized to the intensity of the $[M+H]^+$ peak of the DHB matrix in each spectrum. Each lipid intensity was calculated from the average of ten measurements acquired from three sample replicates. Error bars represent the standard deviation of 30 measurements. AuNP concentration was calculated by dividing Au concentrations (measured by ICP-MS) by the average number of Au atoms in each NP (~200).[5] Even at AuNP concentrations 10-fold higher than those detected in NPSC spleen tissue (represented by the red line at ~600 nM, calculated from Table S1) the particles did not significantly affect lipid ionization, suggesting that all lipid level increases are unrelated to the presence of AuNPs.

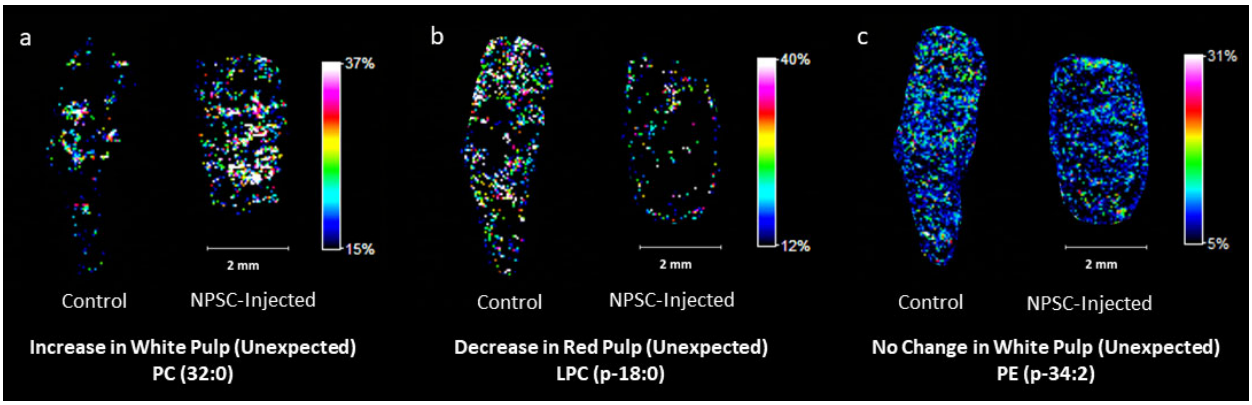

Figure S-7. Example images of lipids that exhibit unexpected changes between the NPSC-injected mouse spleen (in the right of each image set) compared to the control tissue (in the left of each image set).[6] Panel (a) represents an unexpected increase, (b) an unexpected decrease, and (c) and unexpected lack of change between tissues types.

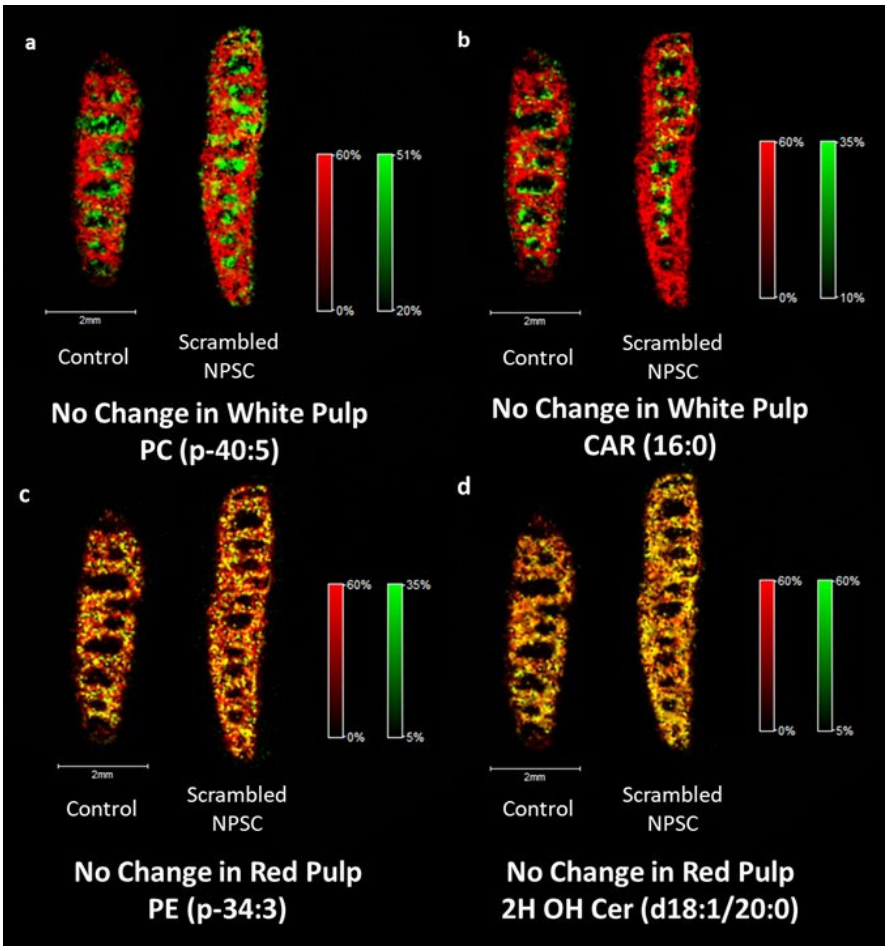

Figure S-8. Example images for scrambled siRNA NPSC-injected mouse spleen tissues. The same lipids that exhibit changes between the TNF-α siRNA NPSC-injected mouse spleen compared to the control tissue in Figure 2 & 3, exhibit no changes between the scrambled siRNA NPSC-injected mouse spleen (in the right of each image set) compared to the control (in the left of each image set).

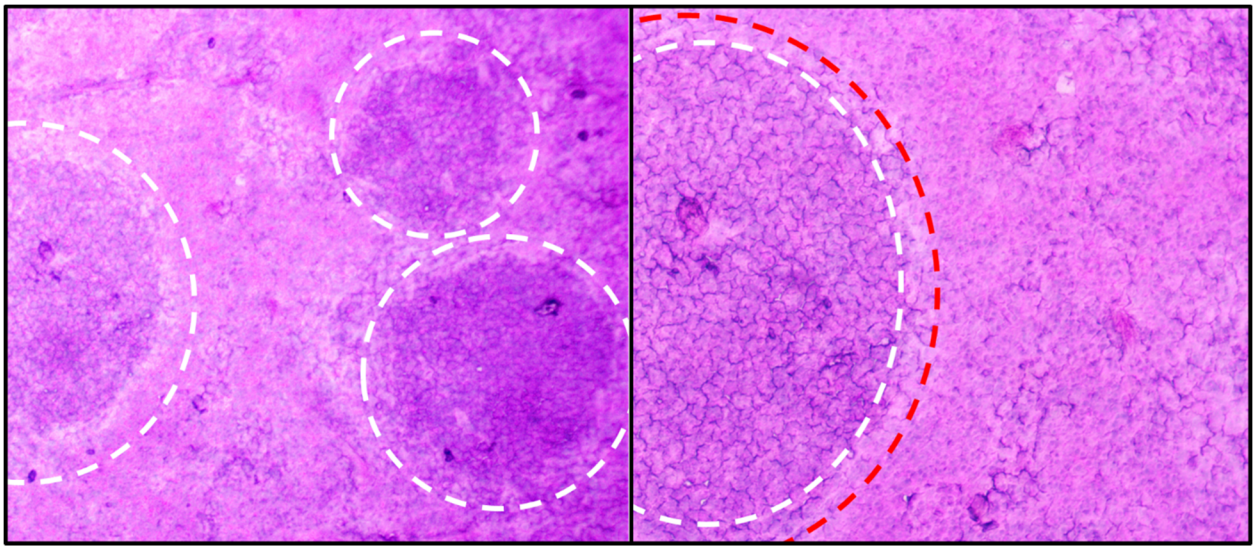

Figure S-9. H&E stain of a mouse spleen tissue, indicating red and white pulp regions. The figure on the left is a representative image of the red and white pulp of a spleen. The white pulp regions are circled in a white dotted outline and the red pulp is the region outside of the dotted lines. The figure on the right is a zoomed in portion of the same spleen tissue shown on the left. The white dotted outline is representative of the white pulp. The region between the red and white dotted outline is the marginal zone. Everything outside of the red dotted line is the red pulp.

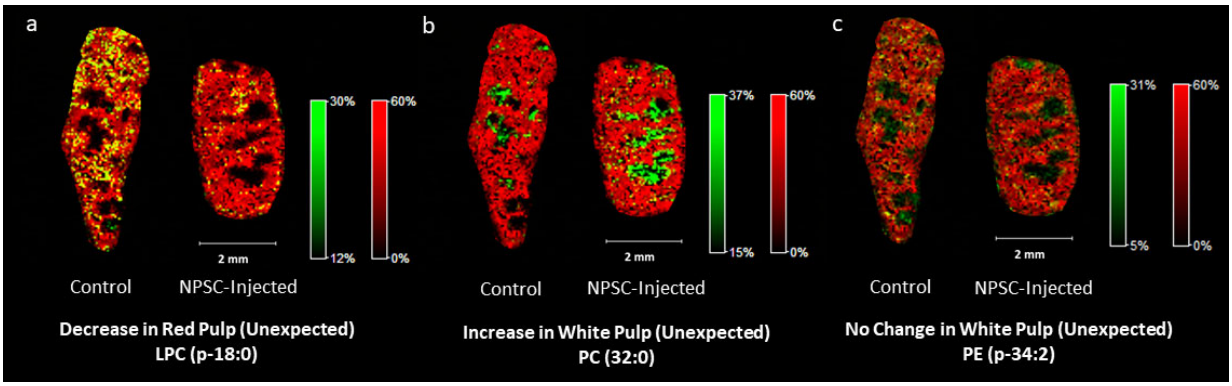

Figure S-10. Example images of lipid responses in NPSC-injected mouse spleen tissues (right in each image pair) compared to control tissues (left in each image pair) with heme B overlays to determine sub-organ distribution. Heme B is indicated by red. Regions of high co-localization between the lipid and heme signals appear in yellow, whereas with low or no co-localization appear in green. Panel (a) is a representative image of lipids that respond to NPSCs in the red pulp of the spleen as indicated by the intense yellow color. In panel (a), 76% of control lipids and 72% of NPSC-injected lipids were colocalized with the heme peaks.

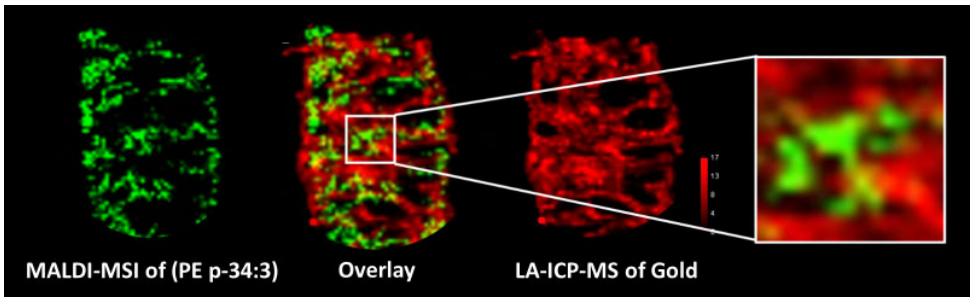

Figure S-11. MALDI-MSI and LA-ICP-MSI overlays of a lipid that is primarily in the red pulp and gold. The low number of yellow pixels indicates that the gold increases are not correlated with the lipid increases in the red pulp.

References

(1) Yang, X.-C.; Samanta, B.; Agasti, S. S.; Jeong, Y.; Zhu, Z.-J.; Rana, S.; Miranda, O. R.; Rotello, V. M. Drug Delivery Using Nanoparticle-Stabilized Nanocapsules. *Angew. Chemie Int. Ed.* **2011**, *50* (2), 477–481.

(2) Brust, M.; Walker, M.; Bethell, D.; Schiffrin, D. J.; Whyman, R. Synthesis of Thiol-Derivatised Gold Nanoparticles in a Two-Phase Liquid–Liquid System. *J. Chem. Soc., Chem. Commun.* **1994**, No. 7, 801–802.

(3) Miranda, O. R.; Chen, H.-T.; You, C.-C.; Mortenson, D. E.; Yang, X.-C.; Bunz, U. H. F.; Rotello, V. M. Enzyme-Amplified Array Sensing of Proteins in Solution and in Biofluids. *J. Am. Chem. Soc.* **2010**, *132* (14), 5285–5289.

(4) Hostetler, M. J.; Templeton, A. C.; Murray, R. W. Dynamics of Place-Exchange Reactions on Monolayer-Protected Gold Cluster Molecules. *Langmuir* **1999**, *15* (11), 3782–3789.

(5) Elci, S. G.; Yan, B.; Kim, S. T.; Saha, K.; Jiang, Y.; Klemmer, G. A.; Moyano, D. F.; Tonga, G. Y.; Rotello, V. M.; Vachet, R. W. Quantitative Imaging of 2 Nm Monolayer-Protected Gold Nanoparticle Distributions in Tissues Using Laser Ablation Inductively-Coupled Plasma Mass Spectrometry (LA-ICP-MS). *Analyst* **2016**, *141* (8), 2418–2425.

(6) Wallace, M.; Morris, C.; O'Grada, C. M.; Ryan, M.; Dillon, E. T.; Coleman, E.; Gibney, E. R.; Gibney, M. J.; Roche, H. M.; Brennan, L. Relationship between the Lipidome, Inflammatory Markers and Insulin Resistance. *Mol. BioSyst.* **2014**, *10* (6), 1586–1595.